Unraveling the multielectron redox reactions of β-$VOPO_4$ for sodium ion batteries

Jiwei Wang, Krystal Lee, M. Stanley Whittingham, and Hao Liu[*]

Department of Chemistry, Binghamton University, Binghamton, New York 13902, United States

ABSTRACT: Realizing multielectron redox reactions is a promising strategy to improve the specific capacity and energy density of rechargeable batteries. Although reversible two-electron redox has been demonstrated for a few cathode materials for Li-ion batteries, few examples are known for Na-ion batteries. Here, we have investigated the multielectron redox of β-$VOPO_4$ for Na-ion intercalation via a combination of X-ray diffraction and absorption spectroscopic methods to elucidate the evolution of crystal and electronic structures during the interaction of more than 1 Na ions per formula unit of $VOPO_4$. The insertion of the second Na ion is possible despite an irreversible structural phase transition to a new, expanded orthorhombic Na_2VOPO_4 phase.

1. Introduction

Intercalation reactions underpin the operation of electrodes for modern, high-energy rechargeable ion batteries. For most intercalation compounds, such as the layered transition metal oxides, the charge storage capacity is limited to one electron redox per transition metal ion center. To further increase the charge storage capacity, it is necessary to extend the limit of intercalation reactions. Enabling multielectron redox, which exploits redox reactions involving more than one electron transfer per transition metal ion center, presents a promising strategy to multiply the charge storage capacity of intercalation electrode materials.[1, 2] Amongst the materials of multielectron redox activity, vanadyl phosphate ($VOPO_4$) has recently been demonstrated for reversible two-electron redox based on the V^{5+}/V^{4+} and V^{4+}/V^{3+} redox couples with the intercalation of 2 Li ions per formula unit (f.u.) of $VOPO_4$.[3-7] While it may appear trivial to adopt this multielectron redox mechanism for the intercalation of other monovalent cations, such as Na^+ ions, it begs the question as to whether and how the lattice can accommodate the large volume change induced by the intercalation of large cations. For example, Na ion intercalation in $FePO_4$ induces an intermediate phase and results in asymmetric charge and discharge processes, neither of which is observed for the Li ion intercalation reaction.[8] This question is further compounded by the rich polymorphism of $VOPO_4$ that could lead to different structural evolution during the intercalation reaction.

Most previous studies on the intercalation of Na into $VOPO_4$ focus on the one-electron redox corresponding to the V^{5+}/V^{4+} redox.[9-12] The reversible intercalation of 1 Na ion per f.u. of $VOPO_4$ has been demonstrated for the layered α_I phase[13] and the β phase.[14] More than one Na intercalation has been reported by Whittingham's group for a K-doped $VOPO_4$ cathode material with the reversible intercalation of 1.66 Na ions per f.u. of $K_{0.36}VOPO_4$.[15] Nonetheless, there is a lack of structural evidence for the intercalation of more than one Na ion into pure $VOPO_4$ phases. A previous study by He et al.[16] showed a long voltage plateau at 1.1~1.2 V with further discharging of β-$NaVOPO_4$, yet this plateau was not mirrored on the subsequent charging cycle and no structural evidence was provided for the $Na_{1+x}VOPO_4$ phase. Using in situ X-ray diffraction and solid state nuclear magnetic resonance spectroscopy, Yang et al.[17] investigated the multielectron reaction of a monoclinic $NaVOPO_4$ and demonstrated the further intercalation of Na ions into the monoclinic $NaVOPO_4$ by activating the V^{4+}/V^{3+} redox couple. However, the structural evolution during the intercalation of the Na ions in the monoclinic $NaVOPO_4$ phase remains unclear. To

elucidate the reaction mechanism of the multielectron redox of $VOPO_4$, it is necessary to understand the structural evolution upon Na-ion intercalation.

Here, we have investigated the multielectron redox of β-$VOPO_4$ as a cathode for Na-ion batteries via a combination of X-ray diffraction and absorption spectroscopic methods to elucidate the evolution of crystal and electronic structures during the intercalation of more than 1 Na ions per f.u. of $VOPO_4$. The insertion of the second Na ion is possible but induces an irreversible phase transition with a substantial structural rearrangement.

2. Experimental section

2.1 **Synthesis of β-$LiVOPO_4$**

β-$LiVOPO_4$ was synthesized through the calcination of a hydrothermally-prepared $LiVOPO_4 \cdot 2H_2O$ precursor following a previous report.[18] In a typical synthesis, 0.909 g V_2O_5 (Sigma-Aldrich, 99.6%), 0.75 g oxalic acid (Sigma-Aldrich, 99.0%), and 3.4 mL phosphoric acid were mixed in 25 mL water and 10 mL ethanol, and then stirred for 18 hours. Subsequently, 2.1g $LiOH \cdot H_2O$ (Sigma-Aldrich) was added to the mixed solution and stirred for an additional 4 hours. The solution was then transferred into a 125 mL Teflon sleeve in a Parr reactor and heated at 160 ℃ for 48 hours. The synthesized products were collected by filtration, washed with water, ethanol, and acetone three times, then dried overnight at 60 ℃ under vacuum. The $LiVOPO_4 \cdot 2H_2O$ precursor obtained from the hydrothermal reaction was annealed at 600 ℃ for 3 hours under flowing O_2 in a tube furnace to yield β-$LiVOPO_4$.

2.2 **Chemical delithiation of β-$LiVOPO_4$**

Chemical extraction of lithium was performed by stirring the β-$LiVOPO_4$ powder in a 0.1M NO_2BF_4 (Sigma-Aldrich) acetonitrile solution under nitrogen for 2 days. 50% excess NO_2BF_4, (corresponding to the molar ratio of 1.5:1 between NO_2BF_4 and β-$LiVOPO_4$) was used to ensure the complete extraction of lithium ions. The products were centrifuged, washed with acetonitrile, and then dried overnight at 70 ℃ under vacuum.

2.3 **Materials characterization**

The elemental analysis was performed with a Varian Vista-MPX Axial inductively coupled plasma (ICP) spectrometer. Scanning electron microscopy (SEM) images and energy-dispersive X-ray spectroscopy (EDX) were acquired with a Zesis FE-SEM Supra-55 VP scanning electron microscope.

X-ray diffraction: The high-resolution X-ray powder diffraction (XRD) data were collected at beamline 11-BM at the Advanced Photon Source (APS), Argonne National Laboratory, with a wavelength of 0.458149 Å. The high-resolution XRD measurement on the electrode (discharged to 4.3V) was conducted at beamline 28-ID-2 at the National Synchrotron Light Source II (NSLS-II), Brookhaven National Laboratory, with a wavelength of 0.1814 Å. TOPAS Academic v6 was used for the structural analysis, including indexing, structure solution via simulated annealing, and structure refinement.[19] Bond valence sum calculation was performed with BONDSTR within the FULLPROF suite.[20]

X-ray absorption spectroscopy: *Ex situ* V K-edge X-ray absorption (XAS) spectra were obtained at beamline 20-BM at APS through a mail-in program. The beamline was operated with a Si (111) double-crystal monochromator. The data were collected in transmission mode and normalized using the Athena software.[21]

2.4 **Electrochemical testing**

The electrochemical properties of the β-$VOPO_4$ were analyzed by using pellet electrodes. The pellet electrodes were prepared by compressing the premixed β-$VOPO_4$, acetylene black, and polyvinylidene fluoride (PVDF) powder in a weight ratio of 5:3:2 with a hydraulic press. CR 2032-coin cells were assembled in an Ar-filled glovebox with the β-$VOPO_4$ pellet as the cathode, Na metal as the anode, and glass fiber as the separator. Different types of electrolytes were used for the electrochemical studies: 1M $NaClO_4$ dissolved in propylene carbonate (PC) and fluoroethylene carbonate (FEC) (98:2 by volume), 1M $NaClO_4$ dissolved in PC without FEC, 1M $NaPF_6$ dissolved in PC and FEC (98:2 by volume), and 1M $NaPF_6$ dissolved in PC without FEC. All the cells were tested with Bio-logic BCS 805 or LAND cyclers.

2.5 **Synchrotron operando XRD measurement**

Operando X-ray diffraction was conducted at beamline 17-BM at the APS with an area detector. Pellet electrode consisting of 60wt% β-$VOPO_4$, 20wt% acetylene black, and 20wt% PVDF was assembled in the AMPIX cell[22] with Na metal as the anode, glass fiber as the separator, and 1M NaClO4 in PC with 2 vol % FEC added as the electrolyte. Diffraction measurements were conducted in the transmission geometry. The diffraction pattern was measured every 12.6 min while the cell was charging at C/20 (1C=165mAh/g) at an elevated temperature (~45 ℃) to improve the Na-ion diffusion.

3. Results and discussion

3. 1 Preparation and characterization of β-$VOPO_4$

The XRD pattern of the as-synthesized β-$LiVOPO_4$ can be indexed to orthorhombic β-$LiVOPO_4$ with a minor β-$VOPO_4$ phase (**Figure S1**).[23] After the chemical delithiation by NO_2BF_4, the powder changes its color from green ($LiVOPO_4$) to yellow ($VOPO_4$) (**Figure S2**). The XRD of the chemically delithiated sample shows β-$VOPO_4$ as the primary phase (99.5wt%) with a minor β-$LiVOPO_4$ phase (0.5wt%) (**Figure 1**A). The unit cell parameters obtained from the Rietveld refinement are a = 7.78632(9) Å, b = 6.13622(7) Å, and c = 6.97232(9)Å, which are in good agreement with the values reported previously.[24] The inset in **Figure 1A** reveals the crystal structure of β-$VOPO_4$ along the b axis. No significant Li is observed in the ICP analysis of the delithiated sample (**Table S1),** which is consistent with the predominant β-$LiVOPO_4$ phase observed in the XRD pattern. The β-$LiVOPO_4$ particles assume a platelet-like morphology with a particle size in the range of 0.5 to 4 μm, consistent with the previous report by He et al.[14] (**Figure 1B**). Similar morphology is observed for β-$VOPO_4$ (**Figure 1C**).[14]

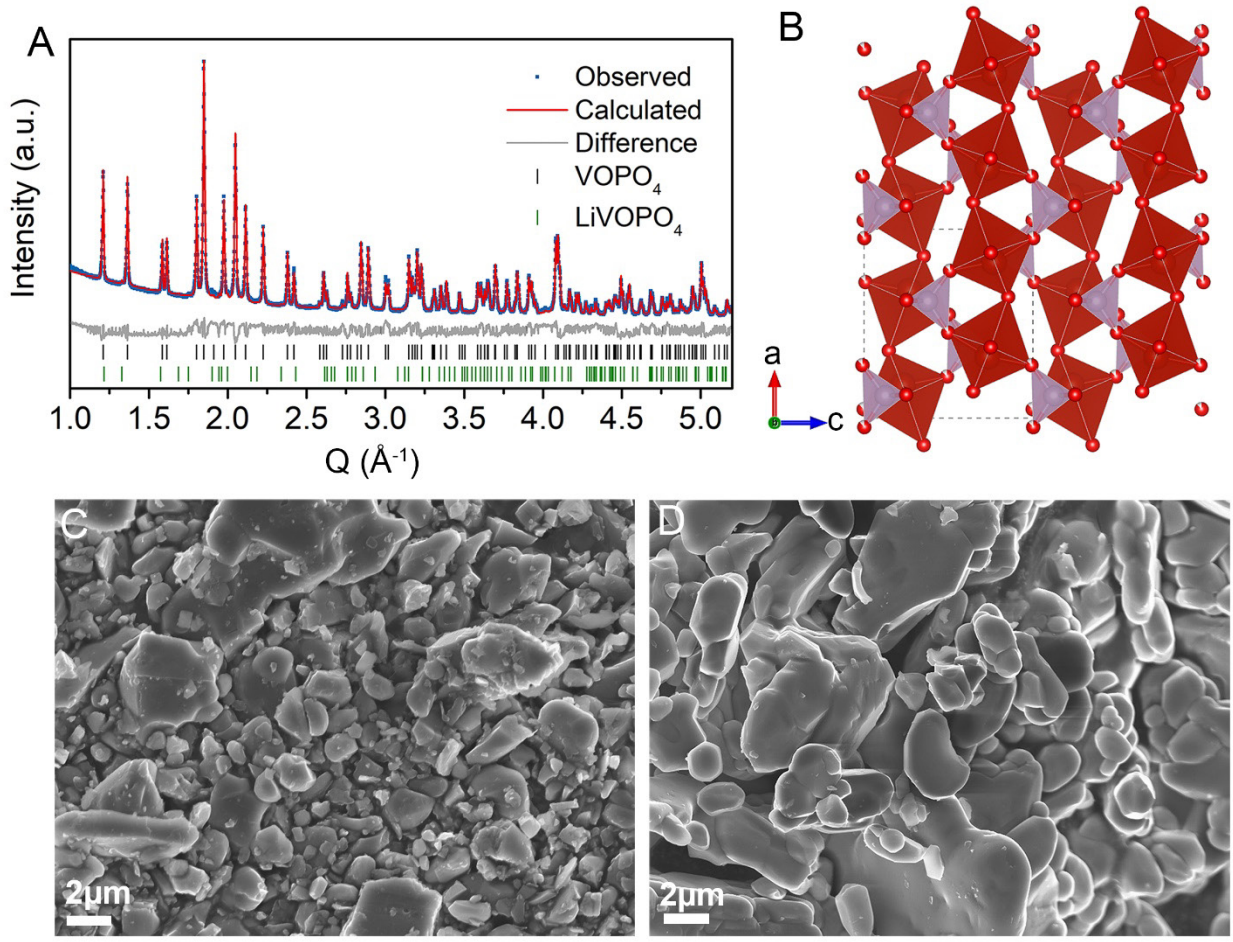

Figure 1*.(A) Rietveld refinement profile for the β-$VOPO_4$ sample obtained by chemical delithiation. The inset shows the structure model of β-$VOPO_4$ projected in the a-c plane. SEM images of (B) the as-prepared β-$LiVOPO_4$ powder and (C) the β-$VOPO_4$ powder obtained by chemical delithiation.*

3.2 Electrochemical cycling of β-$VOPO_4$ with FEC additive

Galvanostatic charge-discharge was first performed to explore the two-electron redox in β-$VOPO_4$ for Na-ion intercalation. Measurements were performed with 1M $NaClO_4$ in PC electrolytes with and without 2vol% FEC additive at 45°C. The temperature was elevated to improve the Na-ion diffusion because the micron-sized β-$VOPO_4$ powder showed a decreased reversible capacity at room temperature due to the long diffusion path (**Figure S3**).

The voltage profile for the electrolyte with FEC additive is shown in **Figure 2A**. Upon discharge (Na-ion intercalation), a long voltage plateau is observed at 3.3V, corresponding to a specific

capacity of 138.1 mAh/g (equivalent to 0.84 Na insertion per formula unit of $VOPO_4$). This voltage plateau is ascribed to the redox couple of V^{5+}/V^{4+} that has been reported previously.[14] Further discharge following the 3.3V plateau resulted in a precipitous drop in voltage until 1.5V, where another plateau is observed. This low voltage plateau delivers a capacity of 90 mAh/g at 1.3V cutoff. While it is tempting to assign this low voltage (<1.5V) reaction to the intercalation of the 2nd Na concomitant with the further reduction of V^{4+}, this voltage range also coincides with the electrolyte side reactions reported for other Na-ion electrodes,[25, 26] thus precluding the unambiguous assignment of this process based on the galvanostatic cycling data alone. The switch from discharge to charge at 1.3V results in a sharp voltage increase to 3.5V, where a voltage plateau of 140 mAh/g is observed. This capacity is equal to the discharge capacity observed for the 3.3V discharge plateau, which suggests that the 3.5V plateau is due to the oxidation of V^{4+} to V^{5+}. It is noted that such a voltage profile is similar to the one reported by He *et al*.[14] Further charge leads to another reaction at 4V that is not observed when the lower cutoff voltage is > 1.5V (i.e., when the low-voltage reaction is not activated, **Figure S4**). Hence, the oxidation reaction at 4V on charge is caused by the reduction reaction at <1.5V.

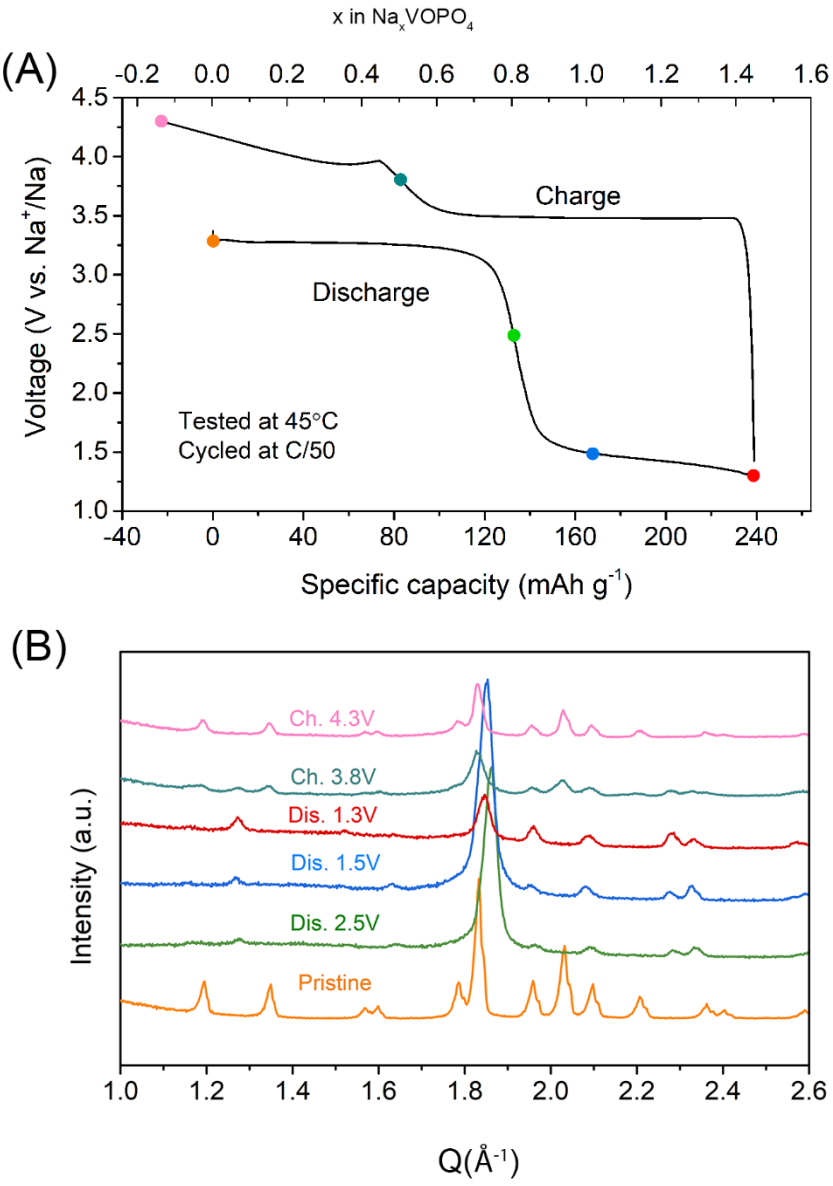

***Figure 2**. (A) Voltage profile of the β-$VOPO_4$ cathode in the electrolyte of 1M $NaClO_4$ with 2% FEC additive. (B) Ex situ XRD patterns of the β-$VOPO_4$ cathode recovered at different states of charge as indicated by solid circles on the voltage profile.*

To determine the nature of the various reactions observed in the voltage profiles, electrodes cycled to different cut-off voltages (**Figure S5**) were harvested and examined by the XRD and XAS. The XRD result (**Figure 2B**) shows the formation of the β-$NaVOPO_4$ phase when discharged to 2.5V, which is consistent with the structural evolution for the first Na-ion intercalation.[14] Nonetheless, no new phases were formed when discharged to 1.3V. The β-$VOPO_4$ phase was partially recovered

upon charging to 3.8V and was fully recovered at 4.3V. The absence of any new phases or significant expansion of the unit cell of the β-$NaVOPO_4$ phase does not support the 2nd Na-ion insertion in β-$NaVOPO_4$. Complementary V K-edge XAS was performed to examine whether the reaction between 1.5 V and 1.3 V during discharge could have resulted in the further reduction of V^{4+} ions in the bulk electrode. (**Figure S6**) The reference spectra measured for $V^{5+}OPO_4$, $LiV^{4+}OPO_4$, and $Li_2V^{3+}OPO_4$ have shown distinct pre-edge and main edge features to allow unequivocal determination of V oxidation state.[5, 27] None of the discharged samples shows any pre-edge peak at 5466.4 eV, which is characteristic of V^{3+}. (**Figure S6A**) Hence, the reaction between 1.5 V and 1.3 V does not correspond to the insertion of the 2nd Na ion in $NaVOPO_4$. To determine whether this reduction reaction 1.5 V is caused by the FEC additive, galvanostatic discharge measurement was performed for an acetylene black electrode in a series of Na-ion electrolytes with and without the FEC additive. (**Figure S7**) It was found that the addition of the FEC additive induces a voltage plateau at 1.5 V that is absent in the electrolyte without FEC. Therefore, the large discharge capacity between 1.5 V and 1.3 V must arise from side reactions with the FEC additive.

3.3 Electrochemical cycling of β-$VOPO_4$ without FEC

To eliminate the side reaction with the FEC, galvanostatic cycling was performed for β-$VOPO_4$ in an electrolyte without the FEC additive. (**Figure 3**) Following the initial discharge plateau at 3.3 V, the voltage drops to 1.5 V, which is similar to the cycling in the electrolyte with the FEC additive. However, the 1.5 V reaction corresponds to only 50mAh/g in capacity and is followed by another voltage plateau at 1V, which suggests the appearance of a new reaction not observed in the cycling with FEC. The subsequent charge profile shows a set of voltage steps at 2 V, 2.5 V and 3.4 V, which resembles the voltage profile for the cycling between $LiVOPO_4$ and Li_2VOPO_4. The charge capacity between 2 V and 3.4 V scales with the discharge capacity observed for the 1 V plateau (**Figure S8**), demonstrating the reaction at 1 V as the origin of the subsequent voltage steps during charge.

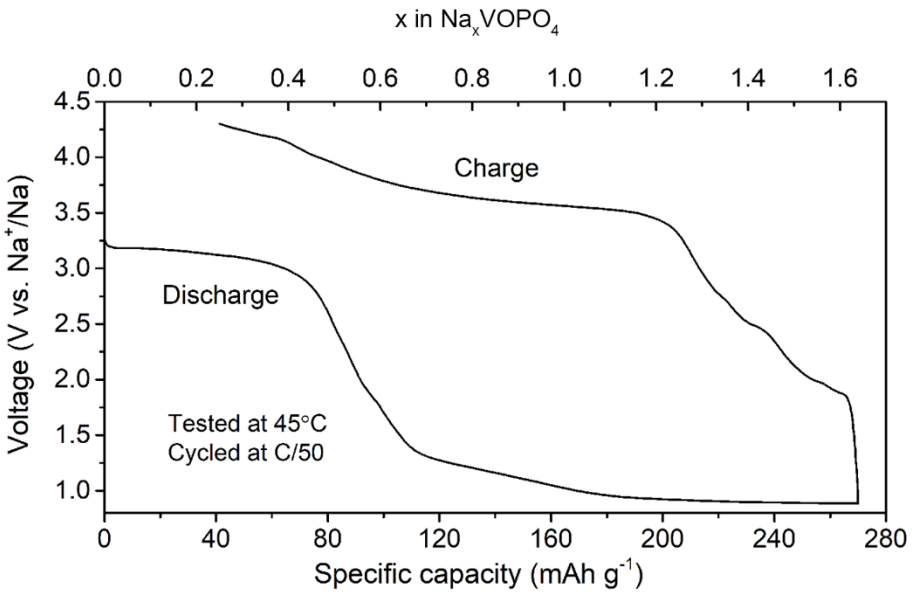

Figure 3. *Voltage profile of the galvanostatic cycling of the β-$VOPO_4$ cathode in a 1M $NaClO_4$ electrolyte in PC without the FEC additive.*

To determine whether the 1 V discharge plateau and the voltage steps on the subsequent charge corresponds to the cycling of the 2nd Na ion in $NaVOPO_4$, synchrotron XRD was performed for electrode samples harvested at the end of discharge (at 275 mAh/g capacity) and at 2.2V, 2.6V and 3.5V upon charge. (The voltage profiles for these samples are shown in **Figure S9**). In addition to the Bragg peaks corresponding to β-$NaVOPO_4$, a new set of Bragg peaks is observed for all samples. (**Figure 4**) This shows that the reaction at 1 V during discharge involves the formation of new crystalline phase(s). Identifying the structure of the newly formed crystalline phases is necessary to unravel the nature of these reactions.

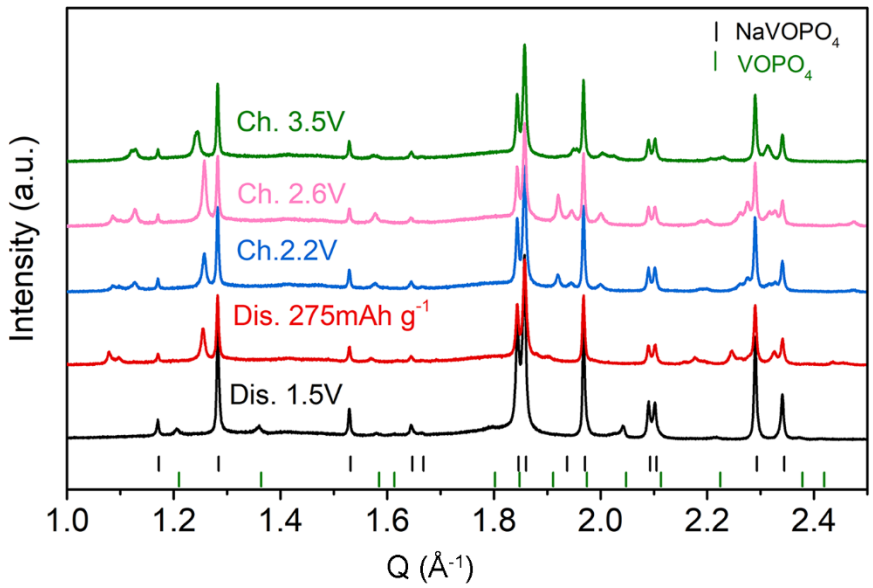

Figure 4. *Ex situ XRD patterns of the cycled β-$VOPO_4$ electrodes recovered at different states of charge. The FEC additive was not used in the electrochemical cycling of these electrodes.*

3.4 Structural studies of the new phases formed during the cycling of the 2nd Na ion

<u>Phases formed during the 1V plateau on discharge</u>: Initial attempts to index all the newly formed peaks to a single phase were not successful. This indicates that the newly formed Bragg peaks arise from more than one phase. We noticed that electrode samples recovered at the same discharge capacity resulted in two different diffraction patterns, where the relative intensities of the first two peaks differ without apparent changes in their peak positions. (**Figure S10**) This suggests that the newly formed peaks result from two phases. Once peaks from the minority phase were excluded, indexing was successful, yielding a unit cell in the *Pnma* space group with a = 5.5459(1) Å, b = 6.58961(9) Å, c = 11.4781(3) Å, and V = 419.40(2) Å^3. An expanded unit cell, where a = 5.5494(3) Å, b = 6.7335(3) Å, c = 11.5280(6) Å, and V = 430.77(3) Å^3 with the same *Pnma* space group, also explains peaks from the other phase. In comparison, the refined unit cell parameters of the β-$NaVOPO_4$ phase are a = 7.53206(8) Å, b = 6.37520(5) Å, c = 7.62751(9) Å, and V = 366.261(6) Å^3. This demonstrates the significant expansion of the unit cell upon the insertion of the second Na ion in β-$NaVOPO_4$.

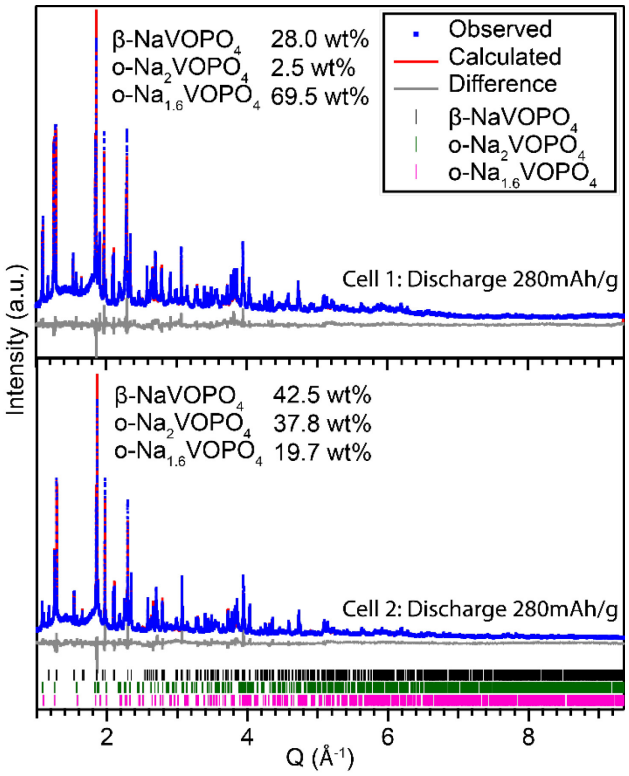

Figure 5. *Fitting profiles for the simultaneous refinement of the β-$NaVOPO_4$, $Na_{1.6}VOPO_4$, and Na_2VOPO_4 phases against two high-resolution synchrotron XRD patterns. Cells 1 and 2 were both discharged to 280 mAh/g in capacity but show different phase compositions, which is likely caused by the different degrees of side reactions between the electrode and the electrolyte below 1.5 V.*

To elucidate the crystal structure of the new phases, the simulated annealing method[28] was employed and successfully yielded an approximant structure model that was further refined. Since none of the XRD patterns contains only a single phase, structures of the two new phases were simultaneously refined against two XRD patterns containing the β-$NaVOPO_4$ and the two new phases. To reduce the number of independent structure parameters, a rigid body constraint was applied to the PO_4 group, where all P-O bonds were identical in length and refined and the O-P-O angle was fixed to the ideal tetrahedral angle of 109.5°. **Figure 5** shows the fitting profiles for the simultaneous refinement of the three phases (β-$NaVOPO_4$ and the two new orthorhombic phases) against the two XRD patterns of the electrode samples harvested from two identical cells discharged to 280 mAh/g in capacity. The refined stoichiometry of the new orthorhombic phase with the larger unit cell is $Na_{2.000}VOPO_4$ (detailed structural information available in **Table S2**),

and this phase is denoted as o-Na_2VOPO_4 (o for orthorhombic). The refined stoichiometry of the new orthorhombic phase with the smaller unit cell is $Na_{1.584}VOPO_4$ (detailed structural information available in **Table S3**), and this phase is denoted as o-$Na_{1.6}VOPO_4$. Since the crystal structures of both phases are similar, only the structure model of the o-$Na_{1.6}VOPO_4$ phase is shown in **Figure 6**(A). The structure model of β-$NaVOPO_4$ is shown in **Figure 6**(B) for comparison. The plausibility of the refined structure was examined by the global instability index (GII) based on the bond valence model. The GII computed by softBV[29] for o-Na_2VOPO_4 is 0.17, which is below the threshold value of 0.2 that indicates structural instability.[30] In comparison, the GII for β-$NaVOPO_4$ is 0.19.

The structure of o-Na_2VOPO_4 is substantially different from β-$NaVOPO_4$ in two aspects: (i) the linear chains of corner-sharing [VO_6] octahedra in the β phase transform into the zig-zag chains of edge-sharing [VO_6] octahedra in the o-Na_2VOPO_4 phase; (ii) each [PO_4] tetrahedron is joined by two corner-sharing [VO_6] and one edge-sharing [VO_6] octahedra in the o-Na_2VOPO_4 phase as opposed to four corner-sharing [VO_6] octahedra in the β phase. This structural rearrangement results in a substantial expansion of the *c* axis (11.5280(6) Å for o-Na_2VOPO_4 as opposed to 7.62751(9) Å for β-$NaVOPO_4$). We note that such a structural transformation is different from the structural changes in a typical intercalation reaction, where the host lattice experiences only minor structural distortions caused by changing bond lengths and angles, such as observed for the transformation between β-$NaVOPO_4$ and β-$VOPO_4$. For the phase transition from β-$NaVOPO_4$ to o-Na_2VOPO_4 to occur, a collective migration of V and O ions must take place to rearrange the structure. Although uncommon, such structural rearrangement upon electrochemical cycling has been reported for the charging of Li_2FeSiO_4, where the monoclinic Li_2FeSiO_4 irreversibly transforms to orthorhombic $LiFeSiO_4$.[31-33]

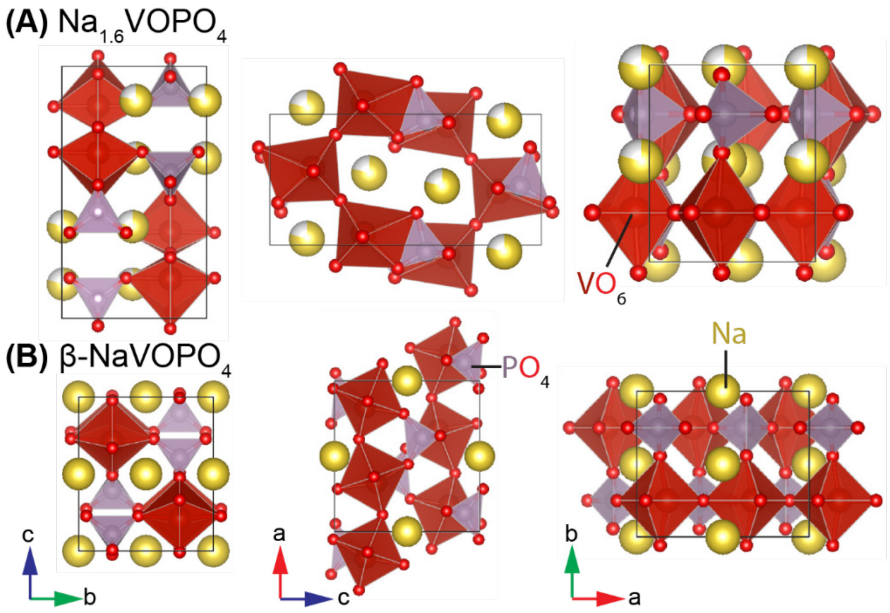

***Figure 6**. Refined crystal structure models of (A) o-$Na_{1.6}VOPO_4$ and (B) β-$NaVOPO_4$.*

<u>Phase formed at 2.2V on charge</u>: The new peaks observed in the XRD pattern for the electrode recovered at 2.2V on charge can be indexed to a monoclinic cell (a = 6.5402(2) Å, b = 5.5493(1) Å, c = 12.9122(6) Å, β = 117.934(4)°, V = 414.03(3) Å^3) in the $P2_1/c$ space group. This monoclinic cell can be obtained through a monoclinic distortion about the a-axis of the o-$Na_{1.65}VOPO_4$ phase and is related to the orthorhombic cell by the transformation in Equation 1 with an origin shift of (1/2, 0, 0). Therefore, the o-$Na_{1.65}VOPO_4$ structure was transformed into the monoclinic cell as the initial structure for the Rietveld refinement. The rigid body constraint was applied to the PO_4 group, where the O-P-O angle was constrained to the ideal tetrahedral angle (109.5 °) and all P-O bond lengths were identical and refined. The rigid body refinement resulted in a satisfactory fitting. (**Figure 7**) The refined structure parameters and the crystal structure model are shown in **Table S4** and **Figure 8**, respectively. The monoclinic distortion leads to two distinct 4e sites for Na with one site fully occupied (Na1 site) and the other half occupied (Na2 site). The half occupied Na2 site is close to the 2d site at (0.5, 0.5, 0), yet refinement with Na2 occupying the 2d site does not lead to any improvement in the goodness of fit. Regardless of the site choice for the Na2 site, the refined occupation of the Na2 site yields the same result that corresponds to $Na_{1.5}VOPO_4$ (denoted henceforth as m-$Na_{1.5}VOPO_4$). This shows that the Na ions are preferentially extracted from every other row of Na ions along the a-axis (b-axis in the orthorhombic structure) during this monoclinic phase transformation.

$$\begin{pmatrix} a \\ b \\ c \end{pmatrix}_{mono} = \begin{pmatrix} 0 & -1 & 0 \\ 1 & 0 & 0 \\ 0 & 1 & 1 \end{pmatrix} \begin{pmatrix} a \\ b \\ c \end{pmatrix}_{ortho} \qquad (1)$$

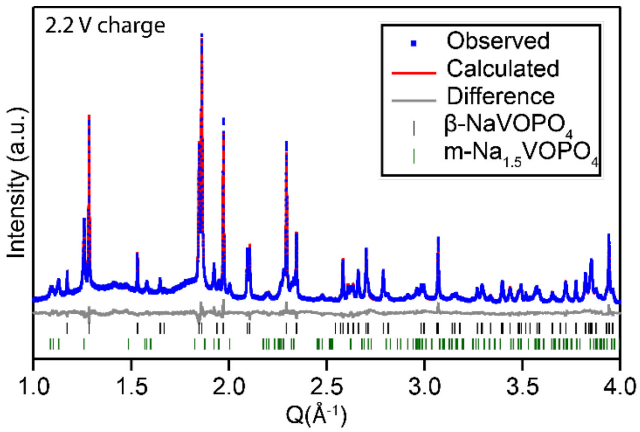

Figure 7*. Fitting profile of the XRD pattern of the electrode at 2.2 V upon charging using Rietveld refinement of an orthorhombic β-$NaVOPO_4$ and a monoclinic $Na_{1.5}VOPO_4$ phases. Only the low Q range is shown.*

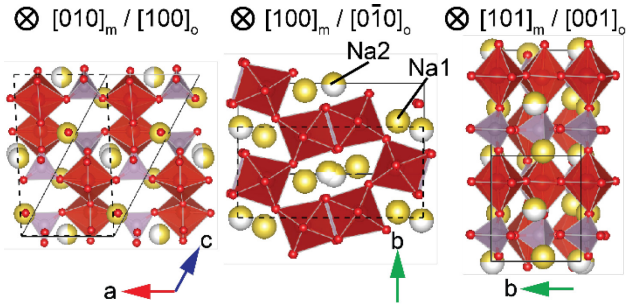

Figure 8*. Refined crystal structure model of the monoclinic $Na_{1.5}VOPO_4$ phase. Dashed lines indicate the unit cell of the distorted orthorhombic cell. $[hkl]_m$ and $[hkl]_o$ correspond to the projection directions defined by the basis vectors of the monoclinic and orthorhombic cells, respectively.*

Phase formed at 2.6V on charge: The XRD pattern measured for the sample obtained at 2.6V on charge is similar to that for 2.2V. (**Figure 9**) Hence, the refined structure of the m-$Na_{1.5}VOPO_4$ phase was adopted as the initial structure for the Rietveld refinement. The refined structure is similar to the 2.2V phase with a slight contraction of the unit cell (a = 6.5369(1) Å, b = 5.5484(1) Å, c = 12.9017(3) Å, β = 117.899(2)°, V = 413.55(2) Å^3). The occupancies of the Na1 and Na2 sites are 0.969(5) and 0.500(4), respectively, corresponding to the stoichiometry of $Na_{1.469}VOPO_4$. This shows that Na ions are preferentially extracted from the Na1 site during charging of the monoclinic phase.

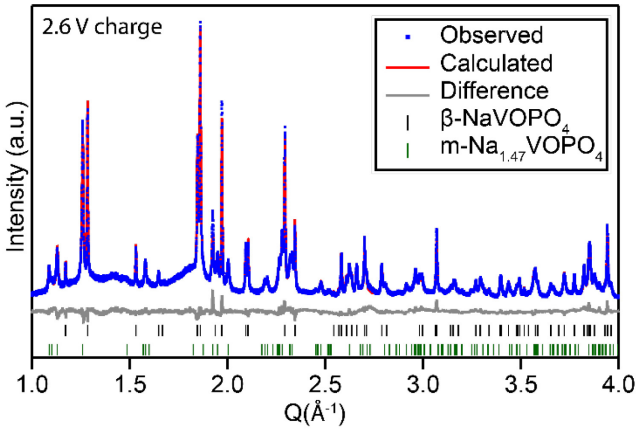

***Figure 9**. Fitting profile of the XRD pattern of the electrode at 2.6 V upon charging using Rietveld refinement of an orthorhombic β-$NaVOPO_4$ and a monoclinic $Na_{1.47}VOPO_4$ phases. Only the low Q range is shown.*

Phases formed at 3.5V on charge: The new phases formed at 3.5V on charge can be explained by two orthorhombic phases with unit cell volumes of 404.95(7) Å^3 and 409.26(5) Å^3. This shows that the monoclinic phase transforms back to the orthorhombic phase with further Na de-intercalation. Rietveld refinement was performed using the o-$Na_{1.65}VOPO_4$ structure as the initial structure model for both phases and resulted in satisfactory fitting result. **(Figure 10)** Yet, the low weight fraction of the new orthorhombic phases and the substantial peak overlap with β-$NaVOPO_4$ did not yield reliable structure parameters, including the Na occupancy.

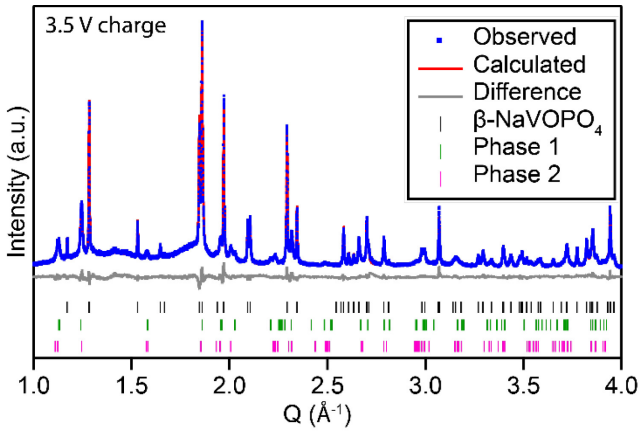

Figure 10. *Fitting profile of the XRD pattern of the electrode at 3.5 V upon charging using Rietveld refinement of an orthorhombic β-$NaVOPO_4$ and two orthorhombic phases (Phase 1 and Phase 2) based on the o-$Na_{1.6}VOPO_4$ structure. Only the low Q range is shown.*

<u>Phase formed at 4.3V on charge</u>: The β-$NaVOPO_4$ phase is completely transformed to β-$VOPO_4$ at 4.3 V, which is expected from the two-phase reaction between β-$VOPO_4$ and β-$NaVOPO_4$ at 3.5 V.[3, 14] In addition to the β phase, the orthorhombic phase with V= 404.45(6) $Å^3$ (i.e., Phase 1 in **Figure 10** for the electrode charged to 3.5 V) is observed. Rietveld refinement was performed using the o-$Na_{1.65}VOPO_4$ structure as the initial structure model. The fitting profile and the refined crystal structure model are shown in **Figure 11** and **Figure 12**, respectively. The refined structure parameters are provided in **Table S6**. Initial refinement yielded a Na occupation of 0.52(1), yet the close proximity between the nearest Na sites, which are separated by ~1 Å, prohibits their simultaneous occupation because of the strong electrostatic repulsion between Na ions at the two sites. Hence, constraint was applied in the refinement to limit the Na site occupancy to be no more than 0.5. The refined Na occupancy corresponds to the stoichiometry of $Na_{1.00(2)}VOPO_4$, and this phase is henceforth denoted as o-$NaVOPO_4$. Unlike the β phase, further Na removal is not realized even at 4.3V for the o-$NaVOPO_4$ phase. (**Figure S11**) The XPS collected from the electrode at 4.3V revealed that the V2p3/2 peak can split into two peaks representing V5+ and V4+. This result can further provide evidence that not all the phases could transfer into β-$VOPO_4$ when charged back to 4.3V.

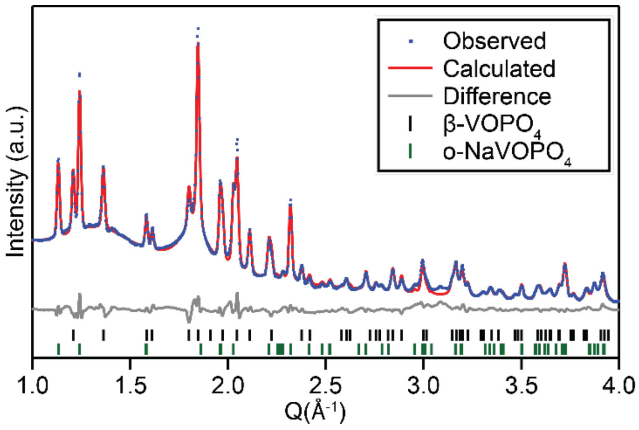

***Figure 11**. Fitting profile of the XRD pattern of the electrode at 4.3V upon charging using Rietveld refinement of a β-$VOPO_4$ and an o-$NaVOPO_4$ phases. Only the low Q range is shown.*

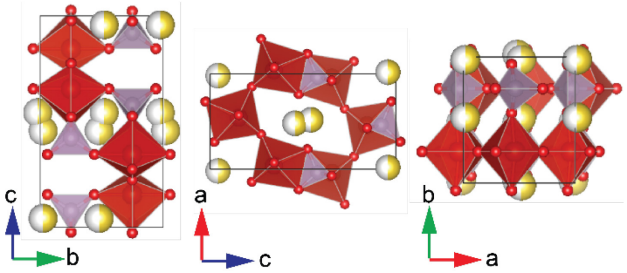

***Figure 12.** Refined crystal structure model of the o-$NaVOPO_4$ phase observed at 4.3 V on charge.*

3.5 Structure analysis of the $Na_{1+x}VOPO_4$ phases

The unit cell volume of the $Na_{1+x}VOPO_4$ phases formed as a result of the insertion of a second Na ion in β-$NaVOPO_4$ is shown in **Figure 13(A)**. The unit cell volume of the $Na_{1+x}VOPO_4$ phases increases monotonically from 404.45 $Å^3$ for x = 0 to 430.77 $Å^3$ for x = 1, which corresponds to a volume expansion of 26 $Å^3$ per intercalated Na per f.u. This is smaller than but comparable to the volume expansion of 33 $Å^3$ observed for the β-$VOPO_4$ phase per intercalated Na.

The average V-O bond length was calculated for the VO_6 octahedral units and increases with increasing Na composition, which is consistent with the reduction of the V ion. (**Figure 13(B)**) The average V-O bond length of the o-$NaVOPO_4$ phase is 1.98 Å, which is similar to the one measured for the β-$Na_{0.93}VOPO_4$ phase by the joint X-ray and neutron diffraction analysis[14] and

is consistent with the +4 oxidation state of the V ion. The average V-O bond length increases to 2.06 Å for o-Na_2VOPO_4, which should only contain V^{3+} based on the chemical formula. In comparison, the experimental V(III)-O bond length reported for ε-Li_2VOPO_4 and H_2VOPO_4 is 2.02~2.03 Å.[34, 35]

The distortion of the VO_6 octahedra is characterized by the standard deviation of the bond lengths, which is shown as the error bar in **Figure 13(B)**. The bond length variation for the o-$NaVOPO_4$ phase is similar to the β-$Na_{0.93}VOPO_4$ phase, which is mainly caused by the formation of the short vanadyl bond for V^{4+} species.[34, 36] The short vanadyl bond is expected to disappear for V^{3+}, which typically forms less distorted VO_6 octahedra. Yet, the refined structure of the o-Na_2VOPO_4 phase still yields a short V-O bond showing a similar level of bond length variation with the o-$NaVOPO_4$ phase. The distortion of the $V^{3+}O_6$ octahedra is likely caused by the edge sharing between the VO_6 and PO_4 polyhedra, where the strong electrostatic repulsion between the V cations and the positively charged P atoms keeps the V ions off centered. Such a distortion has been observed for other transition metal phosphates, such as sodium and potassium iron phosphates,[37-39] where the transition metal and phosphorous polyhedral share a common edge.

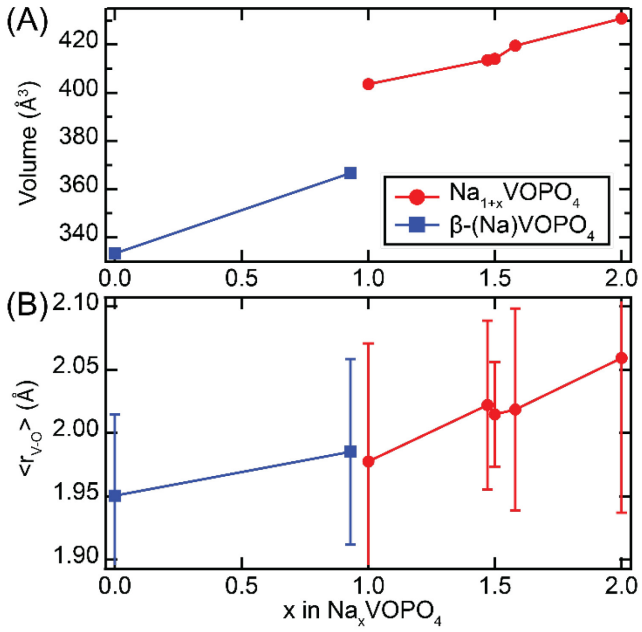

***Figure 13**. (A) Unit cell volume and (B) average V-O bond length of the $Na_{1+x}VOPO_4$ phases formed during the insertion the second Na ion in β-$NaVOPO_4$. Error bars correspond to the*

standard deviation of the V-O bond lengths in the distorted [VO_6] octahedra. Data for the β-$VOPO_4$ and β-$NaVOPO_4$ phases are shown as a comparison and are obtained from reference[34].

To explore the ion diffusion path in the $Na_{1+x}VOPO_4$ phases, the bond valence calculation was used to illustrate the Na-ion diffusion topology. (**Figure 14**) For the o-Na_2VOPO_4 phase, the Na-ion diffusion in the Na channel along the *b* axis follows a square-wave-like path. (**Figure 14A**) This shows that the direct hop along the ion transport direction (*b* axis) is available only through the window enclosed by the PO_4 tetrahedra whereas the window enclosed by the three VO_6 octahedra is too small for Na-ion hopping. This square-wave-like pathway is also observed for the m-$Na_{1.5}VOPO_4$ and o-$NaVOPO_4$ phases. (**Figure 14B** and **C**) For the o-Na_2VOPO_4 and m-$Na_{1.5}VOPO_4$ phases, the BVS map suggests a finite possibility for the Na ions to hop between the Na channels (**Figure 14D** and **F**), whereas this inter-channel hop is forbidden in the o-$NaVOPO_4$ phase. Therefore, the long-range Na-ion transport in the $Na_{1+x}VOPO_4$ phases primarily follows the square-wave-like path along the Na channel. This tortuous diffusion path for the $Na_{1+x}VOPO_4$ phases suggests a lower rate capability than the β-(Na)$VOPO_4$ phase, where Na ions transport via direct hops between Na sites along the diffusion channel.[3, 14]

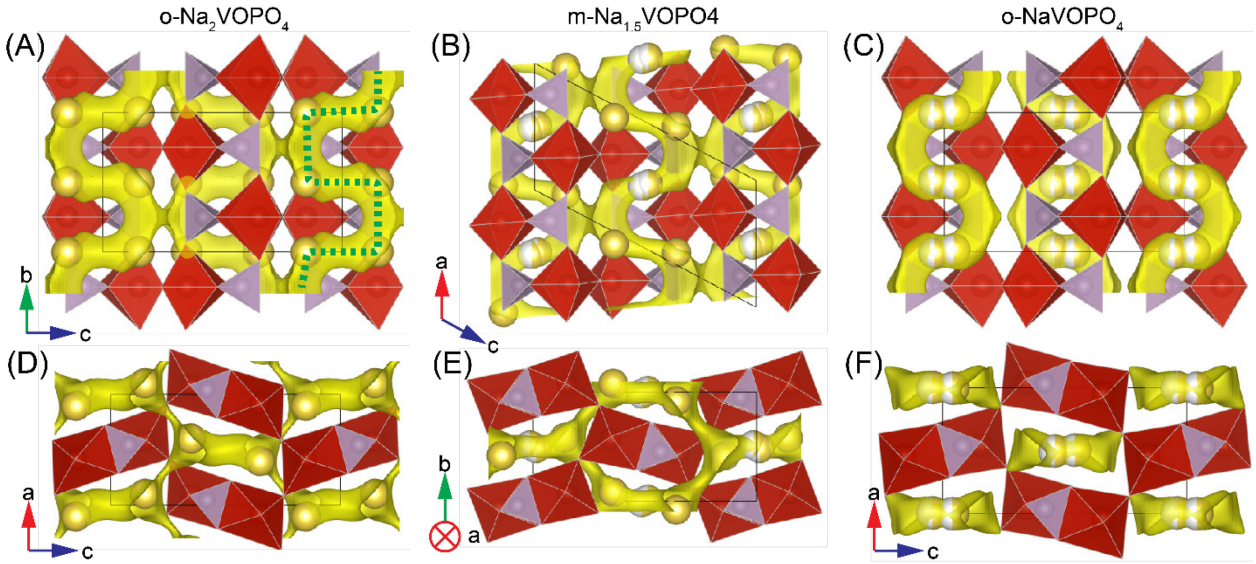

Figure 14. Bond valence sum maps (isovalue 1.5) calculated for (A, D) o-Na_2VOPO_4, (B, E) m-$Na_{1.5}VOPO_4$, and (C, F) o-$NaVOPO_4$. The dotted green trace illustrates the square-wave-like diffusion path of the Na ions.

3.6 Reaction mechanism for cycling of the 2nd Na ion revealed by *operando* XRD

To elucidate the reaction mechanism for the insertion and extraction of the second Na ion in β-$NaVOPO_4$, synchrotron *operando* XRD measurement was performed for the discharge of a β-$NaVOPO_4$ cathode and its subsequent charge process (**Figure 15**). The β-$VOPO_4$ electrode had been discharged to 1.5V at C/20 to form β-$NaVOPO_4$ before the operando XRD measurement (**Figure S12**). The electrolyte used for the *in situ* cell was 1M $NaClO_4$ dissolved in PC with 2 vol% FEC to verify the proposed side reaction observed in the electrochemical cycling in **Figure 2A**. No apparent changes in the XRD patterns are observed during the first ~7 hrs of discharge, where the voltage decreased from 3.32 V to 1.17 V. This confirms that the capacity observed for this voltage window does not come from the Na-ion insertion in the electrode and is attributed to the side reactions involving the electrolyte and the FEC additive.

Following the first 7 hrs of discharge, a new set of peaks (e.g., 2.38° and 2.75° in **Figure 15** and **Figure S13**) appears while the peaks for the β-$NaVOPO_4$ phase decrease in intensity. This new set of peaks corresponds to the o-Na_2VOPO_4 phase identified from the *ex situ* XRD study. This two-phase mixture persists until the end of discharge at 0.86 V with a total discharge capacity (including the side reactions with FEC) equivalent to 1.15 electron transfer per f.u. of $NaVOPO_4$. The discontinuity in the voltage profile at 18.15 hr is caused by the interruption of the *operando* measurement, when the cycling was stopped and the voltage started to increase. By the time the measurement was resumed, the voltage had risen to 1.78V. However, no reaction occurred during this brief interruption, which is evident in the continuity of the *operando* XRD patterns.

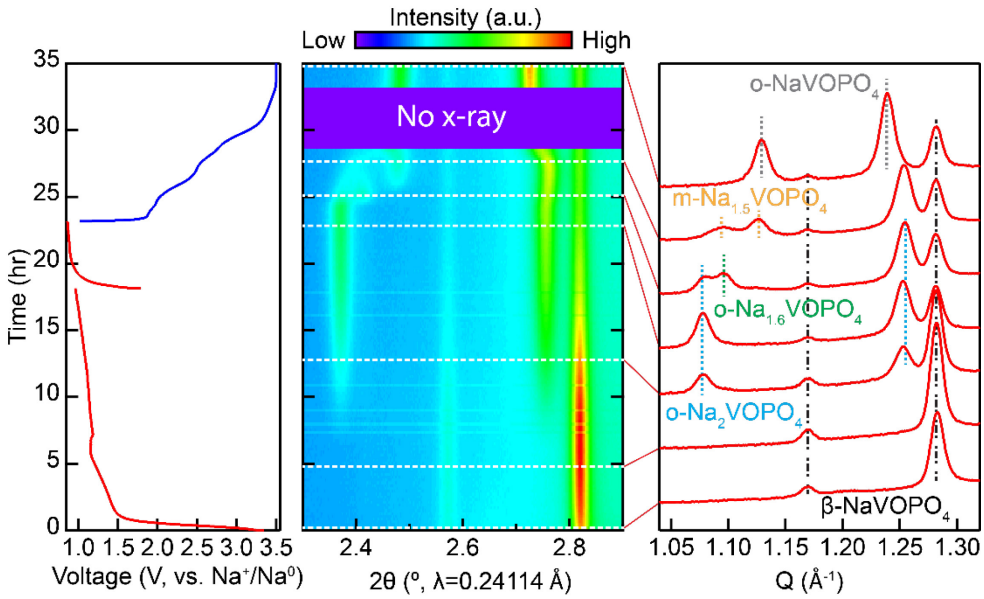

Figure 15*. Operando XRD patterns collected during the discharge of a β-$NaVOPO_4$ cathode and its subsequent charge. The X-ray beam was lost near the end of the charge cycle and is indicated by the violet box.*

Upon charging, Bragg peaks of the o-Na_2VOPO_4 phase begin to disappear with the successive emergence of peaks corresponding to the o-$Na_{1.65}VOPO_4$, the m-$Na_{1.5}VOPO_4$, and the o-$NaVOPO_4$ phases until the end of charge at 3.5V (**Figure 15 right panel**). Meanwhile, no change is observed for the β-$NaVOPO_4$ phase.

Quantitative analysis was performed to track the phase transformation during the insertion and extraction of the second Na ion. (**Figure 16**) Although only the β-$NaVOPO_4$ phase is present in the first 7 hrs of discharge, the refined scale factor, which is proportional to the phase fraction, increases from 30.3×10^{-6} to 34.5×10^{-6} for the β-$NaVOPO_4$ phase, (**Figure 16B**) indicating the continued transformation of a small amount of unreacted $VOPO_4$ phase to the β-$NaVOPO_4$ phase. Further discharge from 7 hr to 23 hr shows a typical two-phase reaction, where the o-Na_2VOPO_4 phase nucleates and grows at the expense of the β-$NaVOPO_4$ phase. (**Figure 16B)** At the end of discharge, 52 mol% of the starting β-$NaVOPO_4$ phase has been transformed to o-Na_2VOPO_4, which requires the charge transfer of 75.3 mAh/g in capacity. However, the specific capacity observed for the discharge from 7 hr to 23 hr corresponds to 116 mAh/g. This shows that only 65% of the discharge capacity contributed to the actual Na insertion in the bulk electrode and significant side reactions took place concurrently with the Na insertion reaction.

Upon charging, the voltage quickly rises to 1.86 V, where a voltage step starts to appear. (**Figure 16F)** Yet, neither the lattice parameters (**Figure 16D**) or the scale factor (**Figure 16E**) of the β-$NaVOPO_4$ and o-Na_2VOPO_4 phases shows significant changes during this voltage step (i.e., during the first hour of charging). This initial voltage step is followed by a second voltage step at 1.97 V, which coincides with the formation of the o-$Na_{1.6}VOPO_4$ phase. The fraction of the o-$Na_{1.6}VOPO_4$ phase increases to a maximum of 25 mol% after 2 hrs of charging, where the slope of voltage profile begins to increase and the monoclinic phase (m-$Na_{1.5}VOPO_4$) emerges. After 4 hrs of charging, this monoclinic phase replaces both the o-Na_2VOPO_4 and o-$Na_{1.65}VOPO_4$ phases. During the growth of the monoclinic phase between 2.6 and 4 hr, the unit cell volume remains effectively constant at 413.9 $Å^3$ except for the very early growth stage. Once the monoclinic phase becomes the dominant phase at 4 hrs into charging, further charging leads to a monotonic decrease in the cell volume of the monoclinic phase to 412.6 $Å^3$ just before the loss of the X-ray beam at 2.74 V. This continuous change in the unit cell volume is characteristic of a single-phase reaction, where the extraction of Na ions is accompanied by the decrease of the Na occupancy rather than the nucleation of a second phase with less Na. This observation is consistent with the *ex situ* XRD result for the phases formed at 2.2V and 2.6V, where a similar unit cell contraction is observed. Therefore, the monoclinic phase is a solid solution and is best described by m-$Na_{1.5-\delta}VOPO_4$, where δ is a small number.

After the restoration of the X-ray beam at 3.5V (10.3 hr into charging), only the o-$NaVOPO_4$ and the β-$NaVOPO_4$ phases are observed. While the exact detail of the phase transition from m-$Na_{1.5-\delta}VOPO_4$ to o-$NaVOPO_4$ is unknown, *ex situ* XRD results suggest that m-$Na_{1.5-\delta}VOPO_4$ probably transforms to the o-$NaVOPO_4$ phase through an intermediate orthorhombic phase with the unit cell volume of 409.26(5) $Å^3$ (Phase 2 in **Figure 10**). Given the time constraint of the *operando* synchrotron experiment, the phase transition for charging above 3.5 V was not measured. However, it can be inferred from the *ex situ* XRD result of the electrode charged to 4.3 V that the o-$NaVOPO_4$ phase is not reactive until 4.3 V and the charging capacity above 3.5 V is attributed to the de-sodiation of the β-$NaVOPO_4$ phase.

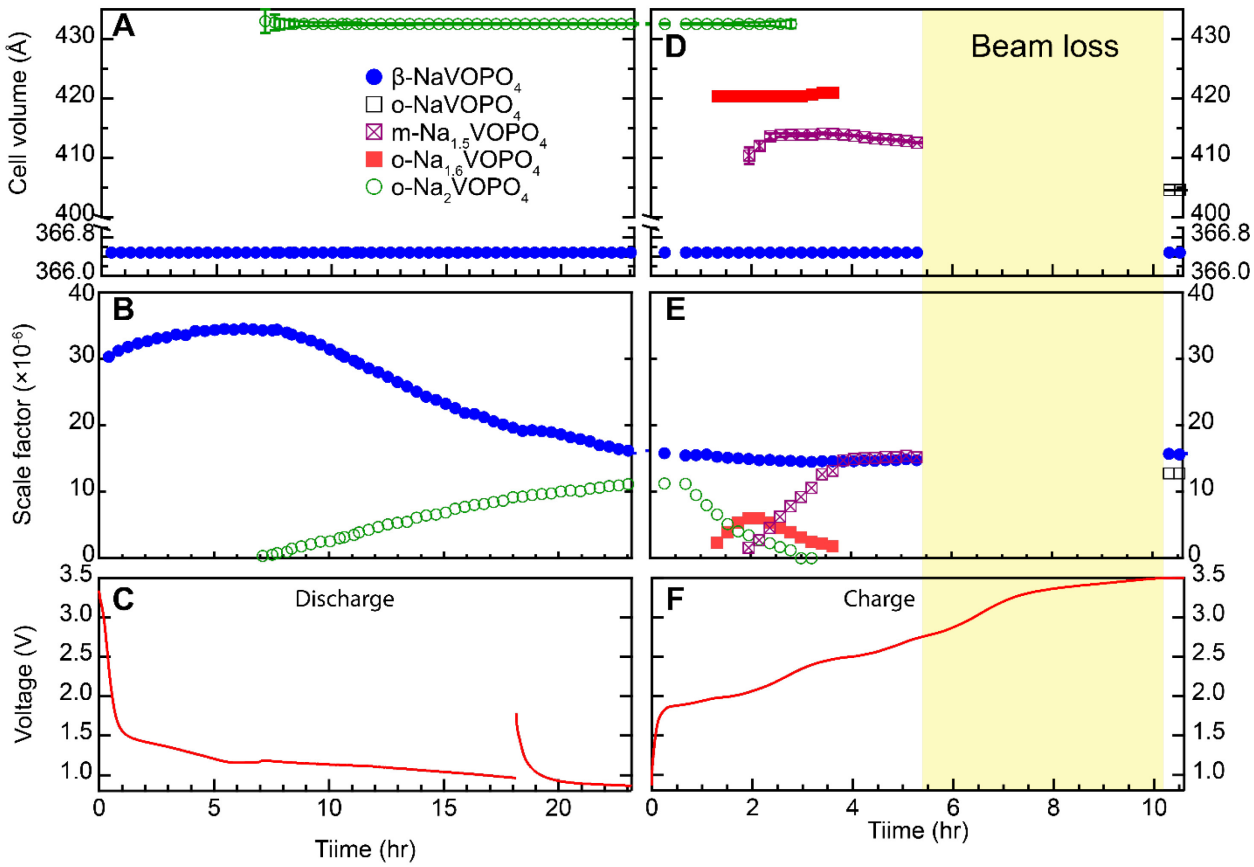

***Figure 16**. Quantitative analysis results of (A, D) the unit cell volume and (B, E) the scale factor of all the phases observed during (C) the discharge and (F) the charge cycle. The period with the X-ray loss is indicated by the region with the yellow shade. Error bars correspond to the estimated standard deviation of the refined parameters.*

3.7 Electrochemical performance of the o-Na_2VOPO_4 cathode

Galvanostatic cycling was performed to evaluate the electrochemical performance of the o-Na_2VOPO_4 phase as a cathode for Na-ion batteries. The o-Na_2VOPO_4 phase was formed by discharging the β-$VOPO_4$ electrode to 250 mAh/g which only allows the partial phase transition from β-$VOPO_4$ to o-Na_2VOPO_4. To evaluate the reversibility of the transformation between o-Na_2VOPO_4 and o-$NaVOPO_4$, galvanostatic cycling was performed with an upper cut-off voltage of 3.5V while keeping a constant discharge capacity of 120 mAh/g. (**Figure 17A**) The initial charge curve shows two voltage steps at 2V and 2.5V, which are mirrored in the discharge profile

with two voltage steps at 2.2V and 1.5V despite a large polarization of 0.5 V. This large voltage polarization corroborates the sluggish Na-ion diffusion in the o/m-$Na_{1+x}VOPO_4$ phases based on the BVS analysis in Figure 14. The same voltage profile is maintained in the subsequent cycles, demonstrating the reversible intercalation reaction between the o-Na_2VOPO_4 and the o-$NaVOPO_4$ phases. (**Figure 17B**).

The partial phase transformation of β-$NaVOPO_4$ to o-Na_2VOPO_4 results in a composite electrode of two electrochemically active phases. To evaluate the electrochemical performance of this composite β-$NaVOPO_4$/o-Na_2VOPO_4 cathode, galvanostatic cycling between 0.9V and 4.3V was conducted to utilize both the redox couple of V^{5+}/V^{4+} for the phase transition between β-$VOPO_4$ and β-$NaVOPO_4$ and the redox couple of V^{4+}/V^{3+} for the phase transition between o-$NaVOPO_4$ and o-Na_2VOPO_4. (**Figure 17C**) It is noted that the theoretical reversible capacity of such a composite electrode is 165 mAh/g and corresponds to the charge storage of $1e^-$ per f.u. of $VOPO_4$ irrespective of the o-$NaVOPO_4$/o-Na_2VOPO_4 phase ratio. The electrode was initially discharged to 275 mAh/g (equivalent to 1.66 Na intercalation per f.u. of $VOPO_4$) to initiate the partial phase transition from β-$NaVOPO_4$ to o-Na_2VOPO_4. In the first charging cycle, the voltage steps at 2V and 2.5V, characteristic of phase transitions between o-$NaVOPO_4$ and o-Na_2VOPO_4, and the voltage plateau at 3.5V, characteristic of the phase transition between β-$VOPO_4$ and β-$NaVOPO_4$, are observed. The charge capacity between 0.9 V and 3.5 V is 80mAh/g, corresponding to the transformation of 24% β-$VOPO_4$ to o-Na_2VOPO_4. However, the voltage plateau corresponding to the phase transition from β-$VOPO_4$ and β-$NaVOPO_4$ at ~3.3V is not observed in the subsequent discharge cycle. It is revealed by the galvanostatic intermittent titration technique that the 3.3V voltage plateau persists but is accompanied by a large voltage polarization. **(Figure S14)** Moreover, the voltage steps between 1.5V and 3.5V disappear after the first cycle, and the charge capacity within this voltage window decreases from 80 mAh/g on the first charge to 53 mAh/g on the second charge and to 40 mAh/g on the third charge. Although the origin of the increased voltage polarization and the disappearance of the voltage steps between 1.5V and 3.5V is not clear and is beyond the scope of the present study, the discharge capacity in the long-term cycling (145.4mAh/g at the 18^{th} cycle shown in **Figure 17D**) is comparable with the theoretical capacity of this composite electrode, which demonstrates the reversible one-electron redox reactions for both the β-$VOPO_4$ and the o-Na_2VOPO_4 phases.

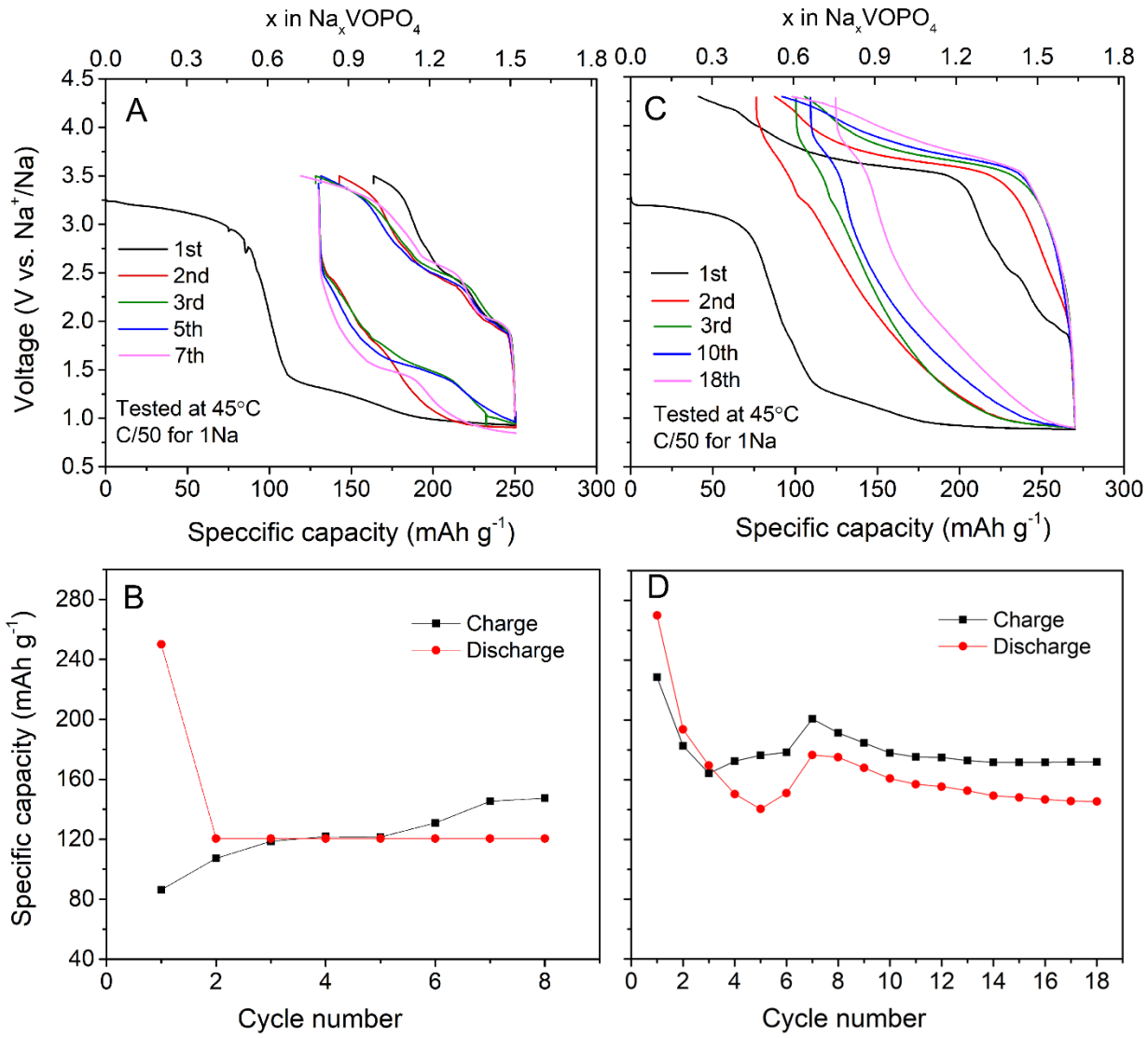

Figure 17. *(A) Voltage profiles and (B) the cycling performance of the β-$VOPO_4$ cathode with an upper cut-off voltage of 3.5V while keeping a constant discharge capacity of 120mAh/g; and (C) voltage profiles and (D) the cycling performance of the β-$VOPO_4$ cathode within the voltage range of 0.9V-4.3V. Both samples were tested at 45℃ with a current rate of C/50 (3.3 mA/g).*

Conclusion

This work shows the prospect of polyanionic compounds as potential candidates for two-electron redox reactions for Na-ion batteries. Through a thorough structural investigation, we have demonstrated the two-electron redox capability of the β-$VOPO_4$ cathode for Na-ion batteries through a reversible Na-ion intercalation to form β-$NaVOPO_4$, followed by an irreversible,

reconstructive phase transition to a new o-Na_2VOPO_4 phase. The Na-ion de-intercalation of the Na_2VOPO_4 phase results in the formation of a series of intermediate $Na_{1+x}VOPO_4$ phases manifested as voltage steps in the voltage profile during charge. However, only one Na ion per f.u. of o-Na_2VOPO_4 can be realized for the upper cut-off voltage of 4.3 V (vs. Na^+/Na^0). Future work is needed to elucidate whether full Na-ion extraction is possible with the o-Na_2VOPO_4 phase and to optimize the electrochemical performance of this electrode material.

AUTHOR INFORMATION

Corresponding Author

*Hao Liu, liuh@binghamton.edu

Author Contributions

The manuscript was written by J.W. and H.L. through the contributions of all authors. J.W. performed the synthesis, materials characterization, the synchrotron XAS and operando XRD experiment, and the analysis of the XAS result. H.L. performed the analysis of the XRD results. K.L. contributed to the materials synthesis. M.S.W. and H.L. supervised the project. All authors have given approval to the final version of the manuscript.

Funding Sources

This research is supported by the Transdisciplinary Areas of Excellence Seed grant, the startup funding of Binghamton University, and New York State Energy Research and Development Authority (NYSERDA).

Notes

The authors declare no competing financial interest.

ACKNOWLEDGMENT

H.L. acknowledges the financial support from Binghamton University's Transdisciplinary Areas of Excellence Seed grant and the startup funding of Binghamton University. J.W. acknowledges the financial support from NYSERDA. This research used resources of the Advanced Photon Source, a U.S. Department of Energy (DOE) Office of Science User Facility operated for the DOE

Office of Science by Argonne National Laboratory under Contract No. DE-AC02-06CH11357. The Beamline 17-BM (GUP-69829), the mail in program of Beamline 11-BM (GUP-81365 and GUP- 79646) and 20-BM (GUP-77757) contributed to the operando XRD, ex situ high-resolution XRD, and XAS data, respectively. The authors acknowledge Dr. Matthew Wahila for the preliminary XAS measurement, Heran Huang for the XPS measurement, and Dr. Jianming Bai for the *ex situ* synchrotron XRD measurement.

REFERENCES

1. Chernova, N. A.; Hidalgo, M. F. V.; Kaplan, C.; Lee, K.; Buyuker, I.; Siu, C.; Wen, B.; Ding, J.; Zuba, M.; Wiaderek, K. M.; Seymour, I. D.; Britto, S.; Piper, L. F. J.; Ong, S. P.; Chapman, K. W.; Grey, C. P.; Whittingham, M. S., Vanadyl Phosphates A_xVOPO_4 (A = Li, Na, K) as Multielectron Cathodes for Alkali‐Ion Batteries. *Adv. Energy Mater.* **2020,** 10, (47), 2002638.

2. Whittingham, M. S.; Siu, C.; Ding, J., Can Multielectron Intercalation Reactions Be the Basis of Next Generation Batteries? *Acc. Chem. Res.* **2018,** 51, (2), 258-264.

3. Lin, Y.-C.; Hidalgo, M. F. V.; Chu, I.-H.; Chernova, N. A.; Whittingham, M. S.; Ong, S. P., Comparison of the polymorphs of $VOPO_4$ as multi-electron cathodes for rechargeable alkali-ion batteries. *J. Mater. Chem. A* **2017,** 5, (33), 17421-17431.

4. Siu, C.; Seymour, I. D.; Britto, S.; Zhang, H.; Rana, J.; Feng, J.; Omenya, F. O.; Zhou, H.; Chernova, N. A.; Zhou, G.; Grey, C. P.; Piper, L. F. J.; Whittingham, M. S., Enabling multi-electron reaction of epsilon-$VOPO_4$ to reach theoretical capacity for lithium-ion batteries. *Chem. Commun.* **2018,** 54, (56), 7802-7805.

5. Wen, B.; Wang, Q.; Lin, Y.; Chernova, N. A.; Karki, K.; Chung, Y.; Omenya, F.; Sallis, S.; Piper, L. F. J.; Ong, S. P.; Whittingham, M. S., Molybdenum Substituted Vanadyl Phosphate ε-$VOPO_4$ with Enhanced Two-Electron Transfer Reversibility and Kinetics for Lithium-Ion Batteries. *Chem. Mater.* **2016,** 28, (9), 3159-3170.

6. Lee, K.; Siu, C.; Hidalgo, M. F. V.; Rana, J.; Zuba, M.; Chung, Y.; Omenya, F.; Piper, L. F. J.; Liu, H.; Chernova, N. A.; Whittingham, M. S., Structure, Composition, and Electrochemistry of Chromium-Substituted ε-$LiVOPO_4$. *ACS Appl. Energy Mater.* **2021,** 4, (2), 1421-1430.

7. Siu, C.; Zuba, M. J.; Zong, Y.; Zhou, H.; Chernova, N. A.; Piper, L. F. J.; Zhou, G.; Whittingham, M. S., Enhanced High-Rate Performance of Nanosized Single Crystal ε-$VOPO_4$ with Niobium Substitution for Lithium-Ion Batteries. *J. Electrochem. Soc.* **2021,** 168, (6), 060519.

8. Moreau, P.; Guyomard, D.; Gaubicher, J.; Boucher, F., Structure and Stability of Sodium Intercalated Phases in Olivine $FePO_4$. *Chem. Mater.* **2010,** 22, (14), 4126-4128.

9. Fang, Y.; Liu, Q.; Xiao, L.; Rong, Y.; Liu, Y.; Chen, Z.; Ai, X.; Cao, Y.; Yang, H.; Xie, J.; Sun, C.; Zhang, X.; Aoun, B.; Xing, X.; Xiao, X.; Ren, Y., A Fully Sodiated $NaVOPO_4$ with Layered Structure for High-Voltage and Long-Lifespan Sodium-Ion Batteries. *Chem* **2018,** 4, (5), 1167-1180.

10. Song, J.; Xu, M.; Wang, L.; Goodenough, J. B., Exploration of $NaVOPO_4$ as a cathode for a Na-ion battery. *Chem. Commun.* **2013,** 49, (46), 5280-2.

11. Ni, Y.; He, G., Stable cycling of β-$VOPO_4$/$NaVOPO_4$ cathodes for sodium-ion batteries. *Electrochim. Acta* **2018,** 292, 47-54.

12. Iffer, E. a.; Belaiche, M.; Ferdi, C. A.; Elansary, M.; Sunar, A. K.; Wang, Y.; Cao, Y., Monoclinic α‐$NaVOPO_4$ as cathode materials for sodium‐ions batteries: Experimental and DFT investigation. *Int. J. Energy Res.* **2020,** 45, (2), 1703-1719.

13. He, G.; Kan, W. H.; Manthiram, A., A 3.4 V Layered $VOPO_4$ Cathode for Na-Ion Batteries. *Chem. Mater.* **2016,** 28, (2), 682-688.

14. He, G.; Huq, A.; Kan, W. H.; Manthiram, A., β-$NaVOPO_4$ Obtained by a Low-Temperature Synthesis Process: A New 3.3 V Cathode for Sodium-Ion Batteries. *Chem. Mater.* **2016,** 28, (5), 1503-1512.

15. Ding, J.; Lin, Y.-C.; Liu, J.; Rana, J.; Zhang, H.; Zhou, H.; Chu, I.-H.; Wiaderek, K. M.; Omenya, F.; Chernova, N. A.; Chapman, K. W.; Piper, L. F. J.; Ong, S. P.; Whittingham, M. S., $KVOPO_4$: A New High Capacity Multielectron Na-Ion Battery Cathode. *Adv. Energy Mater.* **2018,** 8, (21), 1800221.

16. Zhang, Z.; Ni, Y.; Avdeev, M.; Kan, W. H.; He, G., Dual-ion intercalation to enable high-capacity $VOPO_4$ cathodes for Na-ion batteries. *Electrochim. Acta* **2021,** 365, 137376.

17. Liang, Z.; Liu, R.; Xiang, Y.; Zhu, J.; Liu, X.; Ortiz, G. F.; Yang, Y., Electrochemical investigation of multi-electron reactions in $NaVOPO_4$ cathode for sodium-ion batteries. *Electrochim. Acta* **2020,** 351, 136454.

18. Britto, S.; Seymour, I. D.; Halat, D. M.; Hidalgo, M. F. V.; Siu, C.; Reeves, P. J.; Zhou, H.; Chernova, N. A.; Whittingham, M. S.; Grey, C. P., Evolution of lithium ordering with (de)-lithiation in β-$LiVOPO_4$: insights through solid-state NMR and first principles DFT calculations. *J. Mater. Chem. A* **2020,** 8, (11), 5546-5557.

19. Coelho, A. A., TOPAS and TOPAS-Academic: an optimization program integrating computer algebra and crystallographic objects written in C++. *J. Appl. Cryst.* **2018,** 51, (1), 210-218.

20. Rodríguez-Carvajal, J., Recent advances in magnetic structure determination by neutron powder diffraction. *Phys. B: Condens. Matter* **1993,** 192, (1), 55-69.

21. Ravel, B.; Newville, M., ATHENA, ARTEMIS, HEPHAESTUS: data analysis for X-ray absorption spectroscopy using IFEFFIT. *J. Synchrotron Radiat.* **2005,** 12, (4), 537-541.

22. Borkiewicz, O. J.; Shyam, B.; Wiaderek, K. M.; Kurtz, C.; Chupas, P. J.; Chapman, K. W., The AMPIX electrochemical cell: a versatile apparatus forin situX-ray scattering and spectroscopic measurements. *J. Appl. Cryst.* **2012,** 45, (6), 1261-1269.

23. Lee, K.; Zhou, H.; Zuba, M.; Kaplan, C.; Zong, Y.; Qiao, L.; Zhou, G.; Chernova, N. A.; Liu, H.; Whittingham, M. S., Complex defect chemistry of hydrothermally-synthesized Nb-substituted β′-$LiVOPO_4$. *J. Mater. Chem. A* **2023,** 11, (20), 10834-10849.

24. Bustam M. Azmi, T. I., and Yusaku Takita, Cathodic performance of $VOPO_4$ with various crystal phases for Li ion rechargeable battery. *Electrochim. Acta* **2002,** 48, 165-170.

25. Park, S.; Chotard, J.-N.; Carlier, D.; Fauth, F.; Iadecola, A.; Masquelier, C.; Croguennec, L., Irreversible Electrochemical Reaction at High Voltage Induced by Distortion of Mn and V Structural Environments in $Na_4MnV(PO_4)_3$. *Chem. Mater.* **2023,** 35, (8), 3181-3195.

26. Patra, B.; Kumar, K.; Deb, D.; Ghosh, S.; Gautam, G. S.; Senguttuvan, P., Unveiling a high capacity multi-redox ($Nb^{5+}/Nb^{4+}/Nb^{3+}$) NASICON-$Nb_2(PO_4)_3$ anode for Li- and Na-ion batteries. *J. Mater. Chem. A* **2023,** 11, (15), 8173-8183.

27. Rana, J.; Shi, Y.; Zuba, M. J.; Wiaderek, K. M.; Feng, J.; Zhou, H.; Ding, J.; Wu, T.; Cibin, G.; Balasubramanian, M.; Omenya, F.; Chernova, N. A.; Chapman, K. W.; Whittingham, M. S.; Piper, L. F. J., Role of disorder in limiting the true multi-electron redox in ε-$LiVOPO_4$. *J. Mater. Chem. A* **2018,** 6, (42), 20669-20677.

28. Coelho, A. A., Whole-profile structure solution from powder diffraction data using simulated annealing. *J. Appl. Cryst.* **2000,** 33, 899-908.

29. Chen, H.; Wong, L. L.; Adams, S., SoftBV - a software tool for screening the materials genome of inorganic fast ion conductors. *Acta Crystallogr. B* **2019,** 75, 18-33.

30. Garcı; x; a-Muñoz, J. L.; Rodrı; x; guez-Carvajal, J., Structural Characterization of $R_2Cu_2O_5$ (R = Yb, Tm, Er, Y, and Ho) Oxides by Neutron Diffraction. *J. Solid State Chem.* **1995,** 115, (2), 324-331.

31. Masese, T.; Tassel, C.; Orikasa, Y.; Koyama, Y.; Arai, H.; Hayashi, N.; Kim, J.; Mori, T.; Yamamoto, K.; Kobayashi, Y.; Kageyama, H.; Ogumi, Z.; Uchimoto, Y., Crystal Structural Changes and Charge Compensation Mechanism during Two Lithium Extraction/Insertion between Li_2FeSiO_4 and $FeSiO_4$. *J. Phys. Chem. C* **2015,** 119, (19), 10206-10211.

32. Masese, T.; Orikasa, Y.; Tassel, C.; Kim, J.; Minato, T.; Arai, H.; Mori, T.; Yamamoto, K.; Kobayashi, Y.; Kageyama, H.; Ogumi, Z.; Uchimoto, Y., Relationship between Phase Transition Involving Cationic Exchange and Charge–Discharge Rate in Li_2FeSiO_4. *Chem. Mater.* **2014,** 26, (3), 1380-1384.

33. Masese, T.; Orikasa, Y.; Mori, T.; Yamamoto, K.; Ina, T.; Minato, T.; Nakanishi, K.; Ohta, T.; Tassel, C.; Kobayashi, Y.; Kageyama, H.; Arai, H.; Ogumi, Z.; Uchimoto, Y., Local structural change in Li_2FeSiO_4 polyanion cathode material during initial cycling. *Solid State Ion.* **2014,** 262, 110-114.

34. Bianchini, M.; Ateba-Mba, J. M.; Dagault, P.; Bogdan, E.; Carlier, D.; Suard, E.; Masquelier, C.; Croguennec, L., Multiple phases in the ε-VPO_4O–$LiVPO_4O$–Li_2VPO_4O system: a combined solid state electrochemistry and diffraction structural study. *J. Mater. Chem. A* **2014,** 2, (26), 10182-10192.

35. Chen, Y.; Lee, K.; An, K.; Yu, D.; Zhou, H.; Stanley Whittingham, M., Neutron diffraction probing hydrogen in monoclinic H_2VOPO_4. *Mater. Lett.* **2023,** 348, 134661.

36. M. Schindler, † F. C. Hawthorne,† and W. H. Baur‡, Crystal Chemical Aspects of Vanadium: Polyhedral Geometries, Characteristic Bond Valences, and Polymerization of (VOn) Polyhedra. *Chem. Mater.* **2000,** 12, 1248-1259.

37. B. Lajmi, M. H., M. Ben Amara, Reinvestigation of the binary diagram Na_3PO_4-$FePO_4$ and crystal structure of a new iron phosphate $Na_3Fe_3(PO_4)_4$. *Mater. Res. Bull.* **2002,** 37, 2407-2416.

38. Shinde, G. S.; Gond, R.; Avdeev, M.; Ling, C. D.; Rao, R. P.; Adams, S.; Barpanda, P., Revisiting the layered $Na_3Fe_3(PO_4)_4$ phosphate sodium insertion compound: structure, magnetic and electrochemical study. *Mater. Res. Express* **2019,** 7, (1), 014001.

39. David, R.; Pautrat, A.; Kabbour, H.; Mentre, O., Common Building Motifs in $Ba_2Fe_3(PO_4)_4.2H_2O$, $BaFe_3(PO_4)_3$, and $Na_3Fe_3(PO_4)_4$: Labile Fe^{2+}/Fe^{3+}Ordering and Charge-Dependent Magnetism. *Inorg. Chem.* **2016,** 55, (9), 4354-61.